Title

The Relative Importance of Saturated Silica Sand Interfacial and Pore Fluid Geochemistry on the Spectral Induced Polarization Response

Journal

Journal of Geophysical Research Biogeosciences, 123(5)

ISSN

2169-8953

Authors

Peruzzo, Luca
Schmutz, Myriam
Franceschi, Michel
et al.

Publication Date

2018-05-01

DOI

10.1029/2017jg004364

Peer reviewed

The Relative Importance of Saturated Silica Sand Interfacial and Pore Fluid Geochemistry on the Spectral Induced Polarization Response

Luca Peruzzo, Myriam Schmutz, Michel Franceschi, Yuxin Wu, and Susan S. Hubbard

Abstract

Adsorption at the solid-pore fluid interface is a key mechanism controlling the mobility of nutrients and contaminants in subsurface soils and sediments. The spectral induced polarization (SIP) method has been shown to be sensitive to the quantity and type of adsorbed ions. Extending previous results, we investigated the relevance of pH, solution conductivity, and ion type on the SIP response of saturated silica sand. We also performed adsorption experiments to evaluate whether adsorption plays a relevant role on the effect of saturating solution conductivity and pH. Given their environmental relevance and different electrochemical characteristics, we focused on exploring the influence of Cu^{2+} and Na^{+} adsorption on the SIP signature. The adsorption results confirm the expected and modeled pH influence on the adsorption of both Cu^{2+} and Na^{+}. The measured quadrature conductivity spectra indicate that pH and solution conductivity control the electrical double layer electrochemical state and its capacitive behavior. On the contrary, no appreciable SIP signal changes are associated with ion substitution. The adsorption experiments highlight low values of site occupancy for Na and Cu, which suggests that the effects of pH and fluid conductivity are unrelated to their control on the ion adsorption. We interpret the solution conductivity as a proxy for ionic strength. The relative importance of pH and solution conductivity over ion type helps to further constrain the interpretation of SIP results in field geochemical and biogeochemical characterization and monitoring.

1 Introduction

Soil and shallow sediments both affect and depend on the variety of near-surface processes that significantly impact the presence, mobility, and bioavailability of water, nutrients, and contaminants (Lander & Reuther, 2004). These shallow systems are naturally complex as they include interactions between minerals, microbes, organic material, and dissolved constituents over a range of spatial and temporal scales. These systems are also subjected to numerous anthropogenic impacts, including those associated with agricultural treatments, electronic, and metallurgic industrial waste disposal, intensive animal farming, waste and wastewater disposal, and mining. Many of these activities are associated with contamination from heavy metals, which can lead to biotic stress, including serious illness and even human mortality (Hooda, 2010; Järup, 2003).

Adsorption is the most relevant mechanism that controls heavy metal mobility in shallow subsurface systems (Bradl, 2004). Laboratory adsorption

experiments have been used to investigate the different adsorption affinity between specific types of dissolved chemical species (adsorbate) and solid phases (adsorbents). Typically, the results are expressed and interpreted through an adsorption isotherm (Echeverria et al., 1998). Temperature, pH, presence of other dissolved chemical species that promote chelation and competitive adsorption, adsorbent surface topology, and contact time are all relevant variables for the adsorption reaction kinetics and final thermodynamic equilibrium (Milonjić, 2007).

Desorption reactions are performed using chemical extraction methods, whereby adsorbates originally present in geological samples are determined by the use of extractants (Feng et al., 2005). This method allows a direct and quantitative evaluation of the concentration of the sorbed element or compound and the reversibility of the adsorption process. The resulting estimates are inextricably associated with the characteristics of the analyzed samples, such as mineralogy and organic matter content. Desorption experimental results are typically limited to the analyzed samples, and applications to field investigations must rely on significant assumptions about subsurface physiochemical heterogeneity and dynamics. These limitations motivate the development of new geophysical approaches capable of imaging and monitoring the physicochemical soil variability at the relevant field scale (Atekwana & Slater, 2009; Binley et al., 2015).

Geophysical methods are commonly used to characterize the subsurface hydrogeological heterogeneity in high resolution and in a minimally invasive manner (Rubin & Hubbard, 2005). Geophysical data sets can also be acquired in a time-lapse sense, which permits monitoring of changes in subsurface systems (Binley et al., 2015; Vereecken et al., 2006). Several recent studies indicate the potential of geophysical methods for characterizing and monitoring geochemical reactions and biogeochemical processes (Chen et al., 2012, 2013; Hubbard et al., 2008; Revil et al., 2010). In particular, interest has grown in the use of induced polarization (IP) methods for the investigation of geochemical and biogeochemical properties (Revil & Skold, 2011; Vaudelet et al., 2011a; Weller & Slater, 2012; Wu et al., 2010).

The IP method measures the low-frequency electrical properties of geological media through the application of an external electric field and measurement of the capacitive response. While the IP method has long been used for mining exploration, its use in environmental studies is more recent (Atekwana & Slater, 2009; Revil et al., 2015). Using time- or frequency-domain approaches, IP measurements can be obtained over a range of time or frequencies. Frequency-domain investigations produce a spectrum of capacitive responses, a method referred to as spectral induced polarization (SIP) (Revil et al., 2015). The SIP method directly measures the polarization of the medium at the different investigated frequencies, which permits exploration of polarization mechanisms (Kemna et al., 2012).

Laboratory studies have reported changes in the SIP responses associated with the adsorption of different cations onto silica sand, where changes were measured while changing both type and concentration of the dissolved salts (Vaudelet et al., 2011a, 2011b; Weller et al., 2011). These studies revealed relationships between the type of cations and the measured IP capacitive effects. The relationships were interpreted on the basis of the different adsorption behaviors of the dissolved ions and their subsequent impacts on the electrical double layer (EDL) properties, such as charge density and mobility. For this reason, theoretical IP models rely on existing surface complexation models for prediction of the required information on the EDL (Leroy & Revil, 2004; Revil, 2013; Vaudelet et al., 2011b). While complexation models and related adsorption constants have been the subject of substantial research, a significant uncertainty often prevails in practice. As such, combining experimental results with theoretical models has the potential to significantly improve understanding of the IP sensitivity to adsorption processes.

The main goals of this work were to perform laboratory experiments supported by modeling to:

1. investigate the effect of monovalent (Na^+) and divalent (Cu^{2+}) ion concentration, pH, and solution conductivity on the SIP response of saturated silica sand;

2. evaluate whether counterion adsorption plays an important role on the SIP signal sensitivity to the investigated chemical variables; and

3. combine the SIP measurements with laboratory-based chemical data to strengthen the interpretation of the SIP results.

We use copper and sodium in our laboratory experiments for the following reasons. Copper was chosen for its worldwide environmental relevance (Hooda, 2010). For example, subsurface copper accumulation can occur as a consequence of long-term Cu fungicide treatments in agriculture as the result of industrial emissions and urban development (Brun et al., 1998, 2001; Lander & Reuther, 2004). In order to establish a realistic range of copper content for the experiments, we performed chemical extraction experiments on samples taken from a vineyard in the Bordeaux area that had long been subject to Cu fungicide treatment. Sodium was chosen for two reasons: its high content in natural waters and subsequent relevance on biochemical processes (McBride, 1994) and due to growing concern over soil salinity and sodicity (Abrol et al., 1988). Na and Cu were also chosen because of their different adsorption affinity and posited influence on the SIP response (see section 2).

We used silica as the adsorbent substrate because of its natural relevance as a main soil constituent. Given the extensive available literature on silica interfaces, this material represents an ideal adsorbent for mechanistic investigations. Furthermore, silica grains of suitable grain size for

geochemical and SIP studies are readily available and their chemo-physical properties, hardness, and chemical stability in water solution facilitate the experimental procedures.

2 Theoretical Background

2.1 Complexation and Silica-Pore Fluid Interface

Complexation refers to the formation of a complex or a coordination entity resulting from the aggregation of simpler chemical species (such as ions and soluble oxo complexes). In surface complexation, one of the chemical species taking part in the complexation is a surface group, and the resulting complex forms at the solid-liquid interface (Hiemstra, Van Riemsdijk, & Bolt, 1989; Stumm, 1992).

In stable ionic structures, the principle of electroneutrality dictates that the charge of a cation is compensated by the charge of the surrounding anions and vice versa. However, the potential occurrence of crystal irregularities causes the structure to become nonneutral. On the other hand, the neutralization of the ions exposed on the surfaces of a crystal tends to be only partial due to a lower degree of ion coordination (Butt et al., 2004; Hiemstra, Van Riemsdijk, & Bolt, 1989). Consequently, mineral surfaces are in general charged.

The sign and density of the surface charge depend on both solid properties (crystal structure and internal/surface irregularities) and fluid properties (e.g., pH, type, and concentration of ions in solution). When referring to the surface charge, it is convenient to quantitatively define (1) the surface charge per unit of surface area as surface charge density, and (2) the number of surface sites per unit of surface area as surface site density. Ions in solution respond to the surface charge causing the fluid in proximity of the mineral surface to be nonneutral. Ions with opposite charge to that of the surface (counterions) are attracted, while ions with same charge (coions) are forced toward the bulk solution. The resulting structure, including solid surface and charged fluid layer, is called EDL.

Two types of interactions are defined between a mineral surface and the ions in solution: inner-sphere complexation and outer-sphere complexation. In inner-sphere complexation, a direct chemical bonding occurs between the surface group and the adsorbed ion. In the outer-sphere complexation, the interaction between adsorbed ion and mineral surface is electrostatic and the ion remains surrounded by water molecules (i.e., it maintains its hydration shell). Consequently, ions adsorbed through inner-sphere complexation are closer and are more strongly bounded to the mineral surface. On the contrary, the outer-sphere complexation produces a more external layer of ions, called the diffuse layer. For this reason, a widely used model for EDL is the triple layer model (TLM; Stumm, 1992; Yates et al., 1974). In the TLM, three layers are defined as: (1) the solid surface, composed by the surface groups; (2) a layer of chemically strongly bound

ions (inner-sphere complexation); and (3) a more external layer marking the beginning of the diffuse layer (outer-sphere complexation). A stronger adsorption of the divalent ions (here, Cu^{2+}) compared to the monovalent ions (Na^{+}) has been confirmed by laboratory competitive adsorption experiments (Bradl, 2004; Gupta & Bhattacharyya, 2011; Tadros & Lyklema, 1969; Zhu & Alva, 1993), theoretical predictions (Rahnemaie et al., 2006; Sverjensky & Sahai, 1996), and numerical modeling (Porus et al., 2011). In agreement with the literature, we assumed inner-sphere complexation for the Cu adsorption and outer-sphere for the Na ions.

The diffuse layer is described by the Poisson-Boltzmann shown in equation 1. This equation is the combination of the Boltzmann relation (equation 2) and Gauss's law (equation 3), the first linking electric potential and ion concentration, the second the electric field, or electric potential, to the local charge density. The relation between charge density and ion concentration is expressed by equation 4.

$$\nabla^2 \phi = -\frac{1}{\epsilon} \sum_i C_{i\infty} \exp\left[\frac{-z_i F \phi}{RT}\right] z_i F \quad (1)$$

$$C_i = C_{i\infty} \exp\left[\frac{-z_i F \phi}{RT}\right] \quad (2)$$

$$\nabla^2 \phi = \frac{-\rho}{\epsilon} \quad (3)$$

$$\rho_E = \sum_i c_i z_i F \quad (4)$$

For the species i, C_i is the local concentration (mol/L), Z_i is the valence, and $C_{i\infty}$ is the concentration in the bulk fluid (mol/L); F is the Faraday constant $9.65 \cdot 10^4$ (C/mol), R is the universal gas constant 8.32 (J/molK) and T is the temperature in kelvin, φ is the local electric potential (V), ρ_E is the local charge density (C/m^3), and ε is the permittivity (F/m). The Boltzmann relation (equation 1) shows how the attraction/distribution of the ions depends on the ratio of two components: the electric attraction (i.e., $-Z_i\emptyset$) and the chemical diffusion due to the thermal energy (i.e., RT).

A higher surface charge enhances the electric attraction component and ion concentration gradients in the EDL. At the same time, the chemical diffusion component hinders the formation of concentration gradients by smoothing the ion distributions. Lower bulk concentrations are associated to thicker EDL, as described by the Debye length χ.

$$\chi = \sqrt{\frac{\epsilon RT}{2IF^2}} \quad (5)$$

where I is the bulk ionic strength.

Geochemical models can be used to model surface complexation. Among existing models, the Charge Distribution Multisite Complexation model takes into account the possible different adsorption behavior and, on the basis of the TLM, allows both inner- and outer-sphere complexation reactions (Hiemstra & Van Riemsdijk, 1996, 1999; Weerasooriya et al., 2001). In the Charge Distribution Multisite Complexation model, the charge of the surface groups is calculated according to the Pauling rule, whereby the neutralization of a cation in the crystalline structure is distributed over the surrounding ions and vice versa (Pauling, 1929). Then, the charge of a surface group is quantitatively related to the change of ion coordination occurring at the surface. Finally, the reaction constants for the neutralization of the charged surface groups are calculated from the free-energy change associated with the surface complex formation (Hiemstra, Van Riemsdijk, & Bolt, 1989). PHREEQC solves for the overall thermodynamic equilibrium of the solution-surface system, taking into account (1) solution speciation, (2) inner-sphere complexation, and (3) outer-sphere complexation for complete and concurrent neutralization of the surface charge (Parkhurst & Appelo, 2013).

In the case of silica, singly coordinated oxygen molecules (Si-O^-) represent the surface active groups and two protonation reactions occur as

$$\mathrm{Si-O^{-1}} + H_s^+ = \mathrm{Si-OH^0};\ K_{1(6)}$$
$$\mathrm{Si-OH^0} + H_s^+ = \mathrm{Si-OH_2^+};\ K_{2(7)}$$

where K_1 and K_2 are the protonation constants. Silica protonation has been the subject of multiple studies (Hiemstra, Van Riemsdijk, & Bolt, 1989; Sverjensky & Sahai, 1996). The reported values show good agreement for the value of K_1 (LogK_1 = 7.5) and indicate much lower value for K_2. Therefore, the surface species Si-OH^+_2 is a minor species and can be neglected if not in extremely acidic conditions (Behrens & Grier, 2001). The resulting protonation equilibrium determines the surface charge density, which is negative at natural pH conditions and has the Point of Zero Charge (PZC) at pH 2.5.

The other fundamental parameter for the surface charge density is surface site density. When considering only singly coordinated sites, the values reported in most studies range between 5 and 8 sites/nm^2 (Behrens & Grier, 2001; Hiemstra, De Wit, & Van Riemsdijk, 1989; Sverjensky & Sahai, 1996). The presence of ions in solution also affects protonation equilibrium and, consequently, the surface charge. Furthermore, the stronger adsorption of divalent ions compared to monovalent ions produces a higher proton exchange ratio and consequently a more negative surface charge density

(Dove & Craven, 2005; Weerasooriya et al., 2002). Including the assumption of weak adsorption formulation for Na^+, that is, through outer-sphere complexation, allows the numerical simulation of the surface silica protonation equilibria at different pH values with concurrent Na^+ adsorption.

Figure 1 shows the PHREEQC results obtained after calculating the values of the surface charge density of silica over the pH range 3–7 and accounting for the previous theoretical concepts. The values of surface charge density agree with those reported by previous laboratory and modeling studies (Behrens & Grier, 2001; Dove & Craven, 2005; Hiemstra, De Wit, & Van Riemsdijk, 1989). Furthermore, Figure 1 provides insight about the expected variation of the cation adsorption when changing the pH. A higher pH causes silanol groups to deprotonate and consequently develop a more negative surface charge; this will in turn increase the cation adsorption. This has been verified also for Cu^{2+} with specific adsorption experiments (McLaren et al., 1981; Vlasova, 2000; Vuceta, 1976).

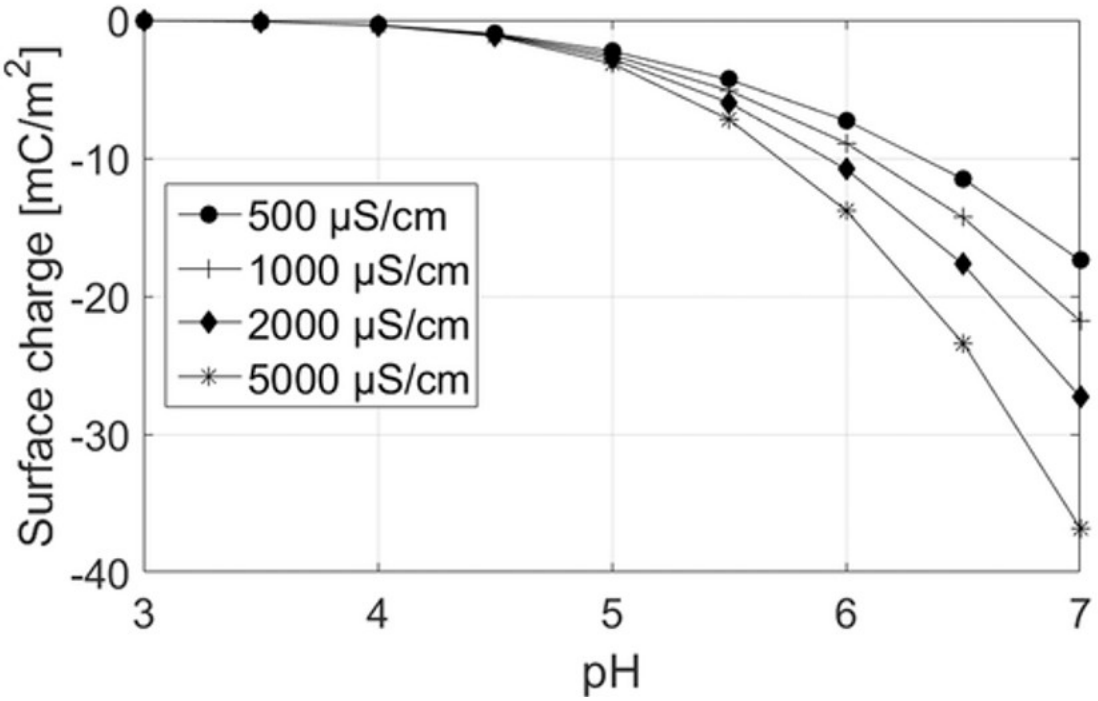

Figure 1

PHREEQC calculation results obtained with CD-MUSIC model of the surface charge density for NaCl solutions with different conductivity and pH value. The pH was adjusted with HCl and $NaSO_4$. Nonspecific adsorption was assumed for the monovalent cation Na^+ and the anions Cl^- and SO_4^{2+}. CD-MUSIC = charge distribution multisite complexation.

2.2 SIP Method

When a low-frequency sinusoidal electric field is applied to a geological media, it induces flow of a sinusoidal electric current. A phase lag is observed between the applied electric field and the measured electrical potential. Consequently, the current can be described considering an in-

phase component, which flows in phase with the applied electric field, and an out-of-phase component, which reflects the presence of polarization mechanisms (Fuller & Ward, 1970).

In order to include the out-of-phase current component, the conductivity of geological media is a complex parameter:

$$\sigma^*(\omega) = \sigma' + i\sigma'' \quad (8)$$

where σ' and σ'' are, respectively, the real (in-phase) and imaginary (quadrature) components of the conductivity (S/m); i is the pure imaginary number and $i^2 = -1$.

The quadrature component is calculated from the phase shift between the injected and measured harmonic electric fields. The following relationships link σ' and σ'' to the phase angle φ (in radian) and the magnitude of the conductivity.

$$\tan\phi = \frac{\sigma''}{\sigma'} \quad (9)$$

$$|\sigma| = \sqrt{\sigma' + \sigma''} \quad (10)$$

Equation 9 highlights how, for a fixed value of σ'', the phase angle φ is inversely proportional to real component σ'. For this reason, the two parameters provide different information and are both considered during the interpretation of the SIP results.

Different induced polarization mechanisms have been suggested, including models that account for the magnitude of the polarization as well as its frequency dependence. Frequency dependence is commonly attributed to either grain size or pore scale size, that is, defining a length of polarization (Binley et al., 2005; Leroy et al., 2008; Tarasov & Titov, 2007; Titov et al., 2002, 2004). An inverse relationship exists between the length of polarization and the frequency. This relationship is most evident when investigating well-sorted geologic materials, where polarization is mostly associated with a specific frequency, called characteristic frequency (peak frequency). Depending on the relative polarization intensity associated with the characteristic frequency, the SIP spectrum may exhibit a well-defined peak or just a corner after which the polarization quickly decreases toward the lower frequencies. For a recent and detailed discussion, see Revil et al., 2015.

A commonly used model that links the SIP results to the adsorption of ions is the Stern polarization model, which considers the movement of adsorbed ions in the Stern layer due to the applied external electric field. Figure 2 shows how the movement of the ions in the Stern layer can produce the formation of electrical dipoles. The adsorbed ions accumulate on the grain side in the direction of the electric pole with opposite charge, creating an

electrical dipole. The Stern polarization arises in the frequency range between a few megahertz and tens of hertz; the frequency of polarization is expected to decrease with increasing grain size (Revil & Florsch, 2010).

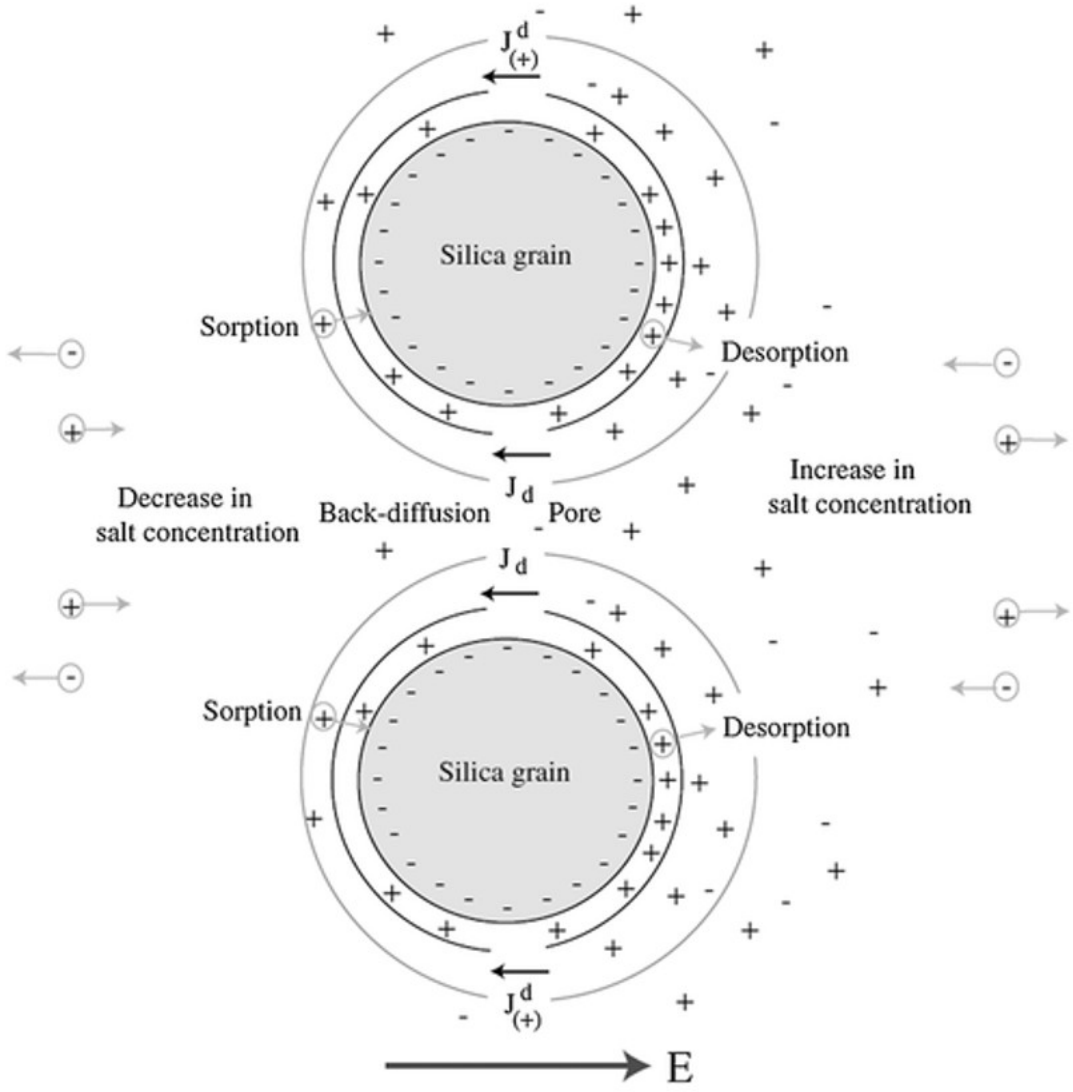

Figure 2

Sketch of the EDL polarization under the influence of an external electric field. The schematic also illustrates of a selective path at the pore throat. Taken from Revil and Florsch (2010). EDL = electrical double layer.

A second SIP model is based on the membrane effect associated with the presence of cation/anion selective paths in the porous media (Revil, 1999; Vaudelet et al., 2011a). This model posits that concentration gradients develop at the sides of the ion-selective paths, which are associated with pore throats. In this model, the extension of the voltage anomaly due to the surface charge becomes the relevant parameter, controlling the formation of the ion-selective paths. Figure 2 shows how the proximity of two grains and

associated EDLs can result in the formation of a selective path and associated electrical dipole.

3 Materials and Methods

3.1 Materials and Experimental Procedure

We prepared 25 separate samples using a commercial silica sand having the following characteristics. The grain-size distribution was characterized through mechanical sieving and compared with the grain-size distribution provided by the manufacturer company (Sibelco France–Sifraco, sand type GA39). The two grain-size distributions indicated a well-sorted, very fine sand (diameter = 90 μm ± 10 μm). The chemical composition of the silica sand was SiO_2 > 99%, Al_2O_3 + K_2O ≈ 1%, and no organic matter was present. We measured the specific surface area with the Brunauer-Emmett-Teller method, the obtained value of 0.2 m^2/g agrees with other reported values for silica sand of the same diameter (Leamson et al., 1969). We calculated the porosity of the samples by measuring the weight difference between saturated weight and dry weight of samples of known volume; the obtained values were consistent at 0.39. The pore fluid solutions were prepared with deionized water and reagent grade chalcanthite ($CuSO_4 \cdot 5H_2O$) and halite (NaCl).

We used 1 kg of sand and 0.5 L of solution for each sample. Sand and solution were placed in a plastic sample holder as shown in Figure 3. The proportion of sand and solution was chosen in order to have sufficient supernatant solution for the chemical analyses. At the same time, the supernatant solution simplified the measurements of pH and fluid conductivity during the adjustment of pH and conductivity of pore fluid, see Figure 3b. After each adjustment, the sand was mixed to enhance the chemical equilibration of pore fluid and supernatant solution. After the mixing, we let the samples equilibrate for 1 day. The use of a hermetic top prevented fluid evaporation and sample contamination during these phases of equilibration. The equilibration was repeated until the desired combination of pH and solution conductivity was obtained, normally 2 or 3 times. We positioned five waterproof threading connectors on the top to allow a correct and reliable positioning of the SIP electrodes and chemical probes. The supernatant solution was removed from the samples and stored for the analyses before the SIP measurements. All the measurements were performed at 20°C.

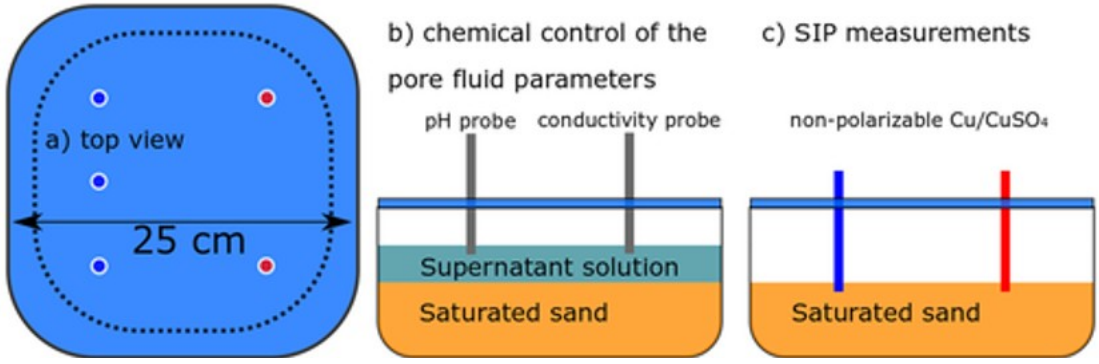

Figure 3

Sample holder and measurement setup. (a) Top view of the sample holder with the positions of the electrodes on the hermetic cover. The three potential electrodes are shown in blue, and the two current electrodes are shown in red. (b) The cross section view shows the positions of the probes used for the measurement of pH and fluid conductivity during the chemical adjustment of the solution. (c) This cross section view shows the positions of the electrodes during the SIP acquisition. The supernatant solution was removed prior to the SIP measurements and analyzed to quantify the adsorption. SIP = spectral induced polarization.

We used inductively coupled plasma mass spectrometry (Thermo Scientific iCAP 6000) to measure the Cu^{2+}, Na^{+}, and Ca^{2+} final concentrations in the removed supernatant solution, and we used an ion chromatography with conductivity detector (Thermo Scientific ICS 900) to measure the Cl^{-} and SO_4^{2-} ion concentrations. The adsorption was calculated by subtracting the final concentration from the known initial concentration of the solution (i.e., before adding the sand). The fraction of surface sites occupied by Na and Cu was calculated on the basis of the adsorption results through the following formula:

$$f_i = \frac{\mathrm{mol}_i \, N_A}{M \, S \, D}, \quad (11)$$

where f_i is the fraction of sites occupied by the adsorbate i, mol_i (mole) is the number of moles adsorbed, N_A is the Avogadro number $6.022 \cdot 10^{23}$ (mole^{-1}), M is the amount of adsorbent (kg), S is the adsorbent specific surface area (m^2/kg), and D is the surface site density of the adsorbent (m^{-2}). Fluid conductivity and pH were measured with a WTW Tetragen 325 conductivity cell and a WTW SenTix 60 electrode.

We used a SIP Fuchs III impedance meter (Radic Research) to acquire the SIP measurements. While the available instrumental frequency range of this system is 1 mHz to 20 kHz, we set the lowest investigated frequency at 5 mHz as no polarization was observed below this value. We used custom built nonpolarizable $Cu/CuSO_4$ electrodes (Abdulsamad et al., 2016; Kremer et al., 2016). Gelatin was added in order to increase the viscosity of the $CuSO_4$solution and, consequently, to avoid the leakage from the electrodes to the sample. Kremer et al. (2016) also included a detailed sketch of the electrodes (see their Figure 2).

The geometrical factor was determined with two approaches: (1) experimentally, tap water of a known conductivity was used as sample (hereafter referred to as “water test”) and the resulting resistance was measured with the impedance meter; (2) numerically, the sample holder and the acquisition geometry were modeled with R3t (Binley, 2013). The geometrical factor values were consistently in the range 0.125 ± 0.0005 (in meter), in good agreement with the numerical estimated value of 0.124.

3.2 Reproducibility and Error

We tested the reliability of the electrodes by monitoring: (1) the impedance response of only water, that is, the values measured during the water tests (e.g., Binley et al., 2005) and (2) the intrinsic potential difference between the electrodes. Observed values were in the range 1 ± 0.2 mV. (3) Upon measuring contact resistance in a tap-water beaker, values were in the range 5 ± 1 k Ohm. Analogous tests on the electrode behavior were performed in Abdulsamad et al. (2016, see their Figure 4) for specific data on the self-potential and potential difference.

We combined the water tests with “resistance tests” to quantify the error associated with the SIP measurements. During the water tests the sample holder was filled only with water. As the water response can be theoretically calculated and subtracted from the measured water test spectra, it is possible to attribute the remaining response to the combined capacitive contribution of electrodes and impedance meter. During the resistance tests, a pure resistance was connected directly to the impedance meter, that is, without the use of electrodes and sample holder. Thus, the resistance test response depends uniquely on the impedance meter. Combining the information from the two types of tests, it is possible to quantify the impedance response associated with the SIP setup and discern the contributions of electrodes and impedance meter.

We performed a water test before the acquisition of the first sample of each set to exclude instrumental drift between the different 4 days of acquisition. Figure 4 shows the results of the four water tests, the pure resistance response, and the water theoretical response. The absolute differences between the theoretical water response and the water tests are smaller than 0.1 mrad up to few kilohertz (0.01 mrad at 1.46 Hz) and associated with the intrinsic response of the impedance meter. Indeed, no significant differences, due to the electrodes and/or sample holder, are visible between the “water + resistance” and the water tests. The observed electrode behavior and SIP resolution agree with other recent studies where the same SIP setup (impedance meter and electrodes) was used (Abdulsamad et al., 2016; Kremer et al., 2016). Kremer et al. (2016, their Figure 3) and Abdulsamad et al. (2016, their Figure 5) also reported similar water test values. On this basis, we find 0.1 mrad to be a proper value for our SIP data resolution.

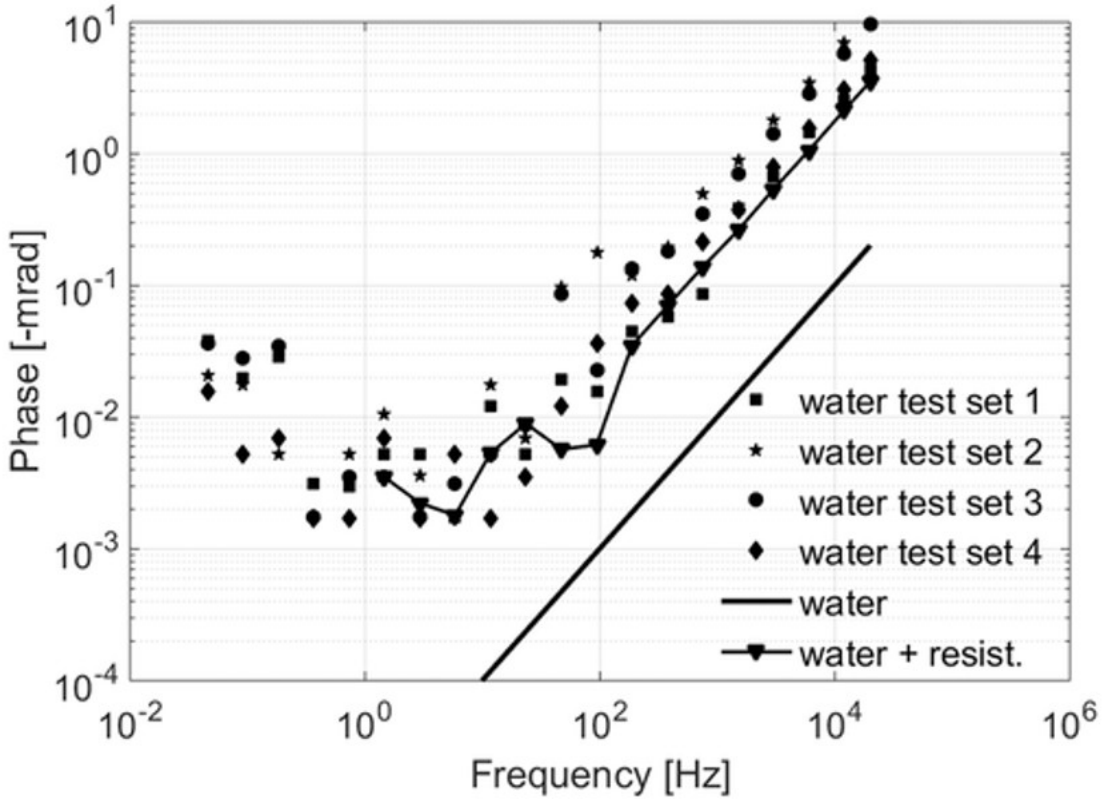

Figure 4

Spectra of the four “water tests” performed prior the acquisition of the four SIP data sets. The “water” trend corresponds to the theoretical response of water due to its electric permittivity. The “water + resistance” data set is the sum of the water response and the spectrum acquire by connecting directly a pure resistance to the impedance meter. The figure shows the absence of relevant and undesired contributions associated with the electrodes and/or other components of our setup. SIP = spectral induced polarization.

3.3 Details on Sample Preparation

We prepared 25 separate samples divided into 4 sets. Using 10 identical sample holders, 10 samples could be prepared at the time. Similar sample holders were used by Schmutz et al. (2010). Set 1 included samples 1–10, Set 2 included samples 11–15; Set 3 included samples 16–20; and Set 4 included samples 21–25. Each set was designed to investigate the effect of a suite of variables.

Set 1 included samples 1–10, this set was designed to investigate the SIP signal changes associated with increasing quantity of dissolved chalcanthite without any fluid adjustments (such as pH or solution conductivity). The set simulated the case of a nonbuffered field contamination and also allowed us to better define what adjustments were relevant for the successive tests. For the solution preparation, only chalcanthite was added in the range 5 to 800 mg/L, corresponding to a concentration of Cu^{2+} between 1.3 and 203 mg/L. Solution conductivity and pH were measured but not adjusted; consequently, they varied with the amount of chalcanthite dissolved (Table 1). The

dissolution of chalcanthite causes hydrolysis; accordingly, the pH decreases as the quantity of dissolved chalcanthite increases.

Table 1. Description of Solution Preparation, Adsorption Data, Calculated Site Occupancy and SIP Results at 1.46 Hz (Peak Frequency) for Each of the 25 Samples of the Four Data Sets

Sample	Solution preparation		Adsorption		Site occupancy		Pore fluid		SIP results at 1.46 Hz		
	Chalcanthite	Halite	Cu	Na	Cu	Na	pH	SC	Phase	In-phase C.	Quadr. C.
Num.	(mg/L)	(mg/L)	(mg/g)	(mg/g)	(%)	(%)		(µS/cm)	(−mrad)	(S/m)	(S/m)
1	5	0	1.25E−3	no halite	0.08	0.00	5.63	6	5.29	2.56E−03	1.35E−5
2	10	0	2.48E−3	no halite	0.16	no halite	5.61	11	4.54	2.73E−03	1.24E−5
3	30	0	6.80E−3	no halite	0.43	no halite	5.54	32	3.99	2.95E−03	1.18E−5
4	40	0	8.87E−3	no halite	0.56	no halite	5.52	41	3.59	3.13E−03	1.12E−5
5	70	0	1.37E−2	no halite	0.87	no hali	5.46	70	2.45	4.41E−03	1.08E−5

Sample	Solution preparation		Adsorption		Site occupancy		Pore fluid		SIP results at 1.46 Hz		
	Chalcanthite	Halite	Cu	Na	Cu	Na	pH	SC	Phase	In-phase C.	Quadr. C.
Num.	(mg/L)	(mg/L)	(mg/g)	(mg/g)	(%)	(%)		(µS/cm)	(−mrad)	(S/m)	(S/m)
						te					
6	100	0	1.79E−2	no halite	1.13	no halite	5.41	97	1.82	4.63E−03	8.43E−6
7	200	0	2.73E−2	no halite	1.72	no halite	5.31	183	1.06	6.71E−03	7.14E−6
8	400	0	3.84E−2	no halite	2.42	no halite	5.20	337	0.53	1.09E−02	5.78E−6
9	600	0	4.20E−2	no halite	2.66	no halite	5.13	477	0.37	1.29E−02	4.77E−6
10	800	0	4.81E−2	no halite	3.04	no hali	5.08	608	0.24	1.86E−02	4.42E−6

Sample	Solution preparation		Adsorption		Site occupancy		Pore fluid		SIP results at 1.46 Hz		
	Chalcanthite	Halite	Cu	Na	Cu	Na	pH	SC	Phase	In-phase C.	Quadr. C.
Num.	(mg/L)	(mg/L)	(mg/g)	(mg/g)	(%)	(%)		(µS/cm)	(−mrad)	(S/m)	(S/m)
						te					
11	0	242	0.00E+0	1.77E−2	0.00	1.55	5.04	540	0.16	1.52E−02	2.49E−6
12	20	234	3.54E−3	1.64E−2	0.22	1.44	4.98	530	0.25	1.43E−02	3.53E−6
13	40	224	6.26E−3	9.77E−3	0.40	0.85	4.99	520	0.28	1.27E−02	3.57E−6
14	100	200	1.17E−2	4.09E−3	0.74	0.36	5.03	520	0.24	1.34E−02	3.25E−6
15	140	188	1.58E−2	1.73E−3	1.00	0.15	5.03	520	0.23	1.29E−02	2.99E−6
16	0	242	0.00E+0	2.21E−2	0.00	1.93	6.02	508	0.35	1.30E−02	4.53E−6

Sample	Solution preparation		Adsorption		Site occupancy		Pore fluid		SIP results at 1.46 Hz		
	Chalcanthite	Halite	Cu	Na	Cu	Na	pH	SC	Phase	In-phase C.	Quadr. C.
Num.	(mg/L)	(mg/L)	(mg/g)	(mg/g)	(%)	(%)		(µS/cm)	(−mrad)	(S/m)	(S/m)
17	20	234	4.92E−3	2.18E−2	0.31	1.91	6.02	506	0.36	1.18E−02	4.21E−6
18	40	224	9.55E−3	2.16E−2	0.60	1.88	6.03	500	0.39	1.21E−02	4.79E−6
19	100	200	2.23E−2	1.86E−2	1.41	1.62	5.98	500	0.35	1.28E−02	4.41E−6
20	140	188	2.99E−2	1.52E−2	1.89	1.33	6.00	520	0.35	1.22E−02	4.33E−6
21	0	70	0.00E+0	6.17E−3	0.00	0.54	5.08	177	0.71	4.25E−03	3.03E−6
22	20	62	4.48E−3	4.49E−3	0.28	0.39	5.05	173	0.72	4.23E−03	3.05E−6
23	40	52	8.06E−3	4.86E−3	0.51	0.42	5.08	165	0.70	4.20E−03	2.95E−6

Sample	Solution preparation		Adsorption		Site occupancy		Pore fluid		SIP results at 1.46 Hz		
	Chalcanthite	Halite	Cu	Na	Cu	Na	pH	SC	Phase	In-phase C.	Quadr. C.
Num.	(mg/L)	(mg/L)	(mg/g)	(mg/g)	(%)	(%)		(µS/cm)	(−mrad)	(S/m)	(S/m)
24	100	26	1.53E−2	2.69E−3	0.96	0.23	5.00	168	0.62	4.22E−03	2.61E−6
25	140	8	1.81E−2	1.65E−3	1.14	0.14	5.00	170	0.54	4.65E−03	2.49E−6

- *Note*. For each sample, 1 kg of silica and 0.5 L of solution were used.

Because of the Ca^{2+} desorption observed in the first data set, for the following three groups of samples the silica was washed twice with acid solution (pH 3) and then rinsed with deionized water until the solution conductivity was lower than 5 µS/cm. In this way we excluded any relevant presence of ions in comparison with the salinities of Sets 2, 3, and 4 (170–500 µS/cm). Note that pH decrease does not promote silica dissolution, which would lead to modifications of the surface topography and, consequently, SIP response. Studies reported that the silica dissolution rate decreases with decreasing pH until the PZC (approximatively 2.5) indicating minimal impact to surface topography (Icenhower & Dove, 2000; Plettinck et al., 1994). Acid wash reduces surface charge on silica sand surface (approaching the PZC), thus facilitating the removal of adsorbed ions, such as Ca. After acid wash, the sand was dried for 1 week at 100 °C.

Sets 2 and 3 (samples 11–15 and 16–20, respectively) were designed to specifically explore the effect of the Cu-Na substitution under realistic field-solution conductivity and pH buffering processes. The pore fluid solution of both sets was adjusted at 500 µS/cm; the pH of Set 2 was adjusted at pH 5 ± 0.05, and the pH of Set 3 was adjusted at pH 6 ± 0.05. Halite was added to adjust the solution conductivity, while HCl and $NaSO_4$ were used to adjust the pH. The HCl solution had pH 1, in this way the amount of solution needed for the sample preparation was small (< 200 µL) and negligible compared to sample solution volume (0.5 L). For the same reason, the $NaSO_4$ solution had pH 10. In order to avoid the copper precipitation as $Cu(OH)_2$, in particular at pH 6, we reduced the maximum amount of chalcanthite dissolved to 140 mg/L. With a concentration of 140 mg/L the copper precipitation occurs at pH 6.3, thus outside the pH measurement uncertainty limit of 6 ± 0.05 (Fu & Wang, 2011; Mirbagheri & Hosseini, 2005). The saturation index was also checked with the PHREEQC software as described below. Solution conductivity and pH were adjusted after adding the sand in order to compensate the effect of adsorption/desorption reactions. The solution pH was adjusted incrementally until the desired value was achieved. The added amounts of HCl and $NaSO_4$ were tabulated and then used for the PHREEQC complexation model calibration along with the other laboratory results.

For Set 4 (samples 21–25), we fixed the solution conductivity at 170 µS/cm in order to better differentiate the effects of pH and solution conductivity. The solution conductivity value was significantly lower compared to the previous sets (from 500 µS/cm to 170 µS/cm); but it also allowed us to maintain the range of Cu concentrations used before (Sets 2 and 3). The pH was adjusted to 5 following the same method described above.

3.4 Modeling With PHREEQC

PHREEQC is a software for geochemical modeling, including speciation, dissolution, and surface complexation (Parkhurst & Appelo, 2013). As the goal of this work was to combine the SIP data with laboratory-based chemical and adsorption information in order to reduce the uncertainty

associated with the geochemical modeling, PHREEQC was used as a support to the laboratory work.

The geochemical modeling was used prior to preparing the solution to properly address difficulties that arise from the physical coupling between pH, Cu concentration, overall solution conductivity, and successive effect of the silica sand. All the different chemical properties of the solution had to be simultaneously adjusted while minimizing the volume changes of the solution itself. The effect of the silica sand mainly affected the pH and was due to the protonation reactions, which in turn depends on the initial pH of the solution. For the pH adjustment, we defined two new chemical species with the electrochemical properties of $NaSO_4$ and HCl (i.e., same properties but different names). In this way, it was possible to separately track the different contributions from pH adjustment and overall solution conductivity. For example, it was possible to distinguish between the Na concentration fraction due to the pH adjustment ($NaSO_4$) and the pore fluid conductivity control (NaCl). This numerical feature represented a detailed starting point for the laboratory solution preparation and allowed us to reduce the number of chemical adjustment, which in turn reduced preparation time and solution volume changes. The model calibration significantly improved the prediction quality and consequently the sample preparation.

The final model was able to fit the Cu and Na adsorption values, while automatically adjusting the pH and the fluid conductivity at the desired values (as shown in Table 2). We highlight that the automatic adjustment is a possible source of error as the final laboratory pH and solution conductivity values commonly presented small discrepancies compared to the desired values (see Table 1). On the other hand, this approach is more favorable, in terms of time and proneness to major error, compared to the manual adjustment of the single reactions, particularly when dealing with numerous data sets.

Table 2. PHREEQC Model Inputs and Calibrated Variables

Surface area	0.2 m^2/g	BET, (Leamson et al., 1969, in particular their Figure 2)
Site density	8 sites/nm^2	(Behrens & Grier, 2001, their Figure 1; Hiemstra, De Wit, & Van Riemsdijk, 1989, their Figure 10)
Inner capacitance, C1	2.5 F^2/m^2	(Hiemstra, De Wit, & Van Riemsdijk, 1989, their Table 1)
Outer capacitance, C2	0.2 F^2/m^2	(Vaudelet et al., 2011b, their section 2.4)
	Log*K* = 7.5	(Hiemstra, De Wit, & Van Riemsdijk, 1989, their Figure 1 and Table 1)
	Log*K* = −2	This work
	Log*K* = −3.2	This work
$Cu(OH)_2 + 2H^+ = Cu^{2+} + 2H_2O$	Log*K* = 8.67	This work, calibration based on the existing literature (Awan et al., 2003; Fu & Wang, 2011; Mirbagheri & Hosseini, 2005)

- *Note*. BET = Brunauer-Emmett-Teller.

The control of the copper hydroxide saturation index was crucial for the final Cu adsorption experiments. If precipitation occurs, its effect could be misinterpreted as adsorption, leading to an overestimation of the amount of Cu removed from solution. Such precipitation could potentially compromise the consistency and correctness of the adsorption experiment results. The Cu saturation concentrations, calculated with the geochemical model for the different pH values investigated, agreed well with the literature and excluded the presence of precipitation reactions (see Table 2). In this sense, Set 3 was of most concern due to its higher pH values. Figure 5 shows that Cu concentration for Set 3 was always below the Cu hydroxide precipitation threshold for a solution pH of 6 (the threshold is indicated by the dashed line). The fact that some samples of Set 1 (i.e., samples 8, 9, and 10) lie beyond the dashed line does not imply precipitation as their pH is significantly lower than 6 and the concentrations associated with the precipitation are consequently higher.

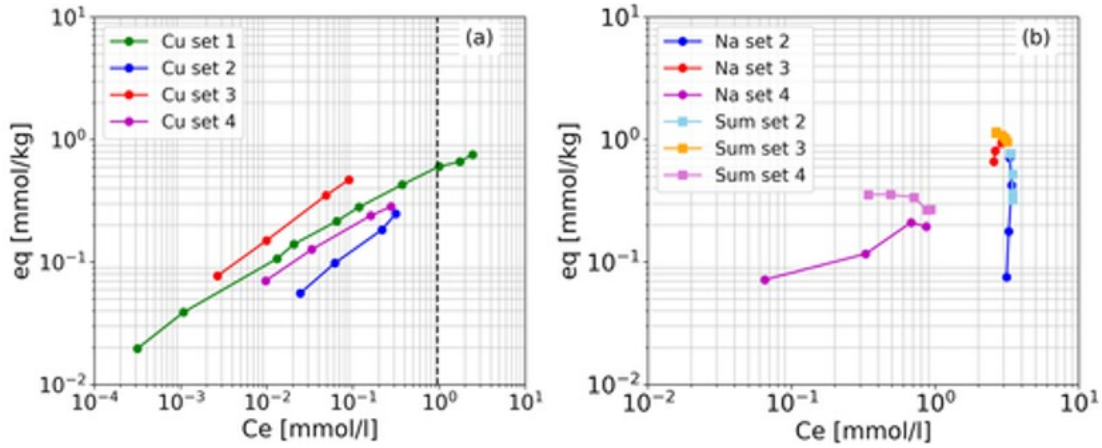

Figure 5

(a) Adsorbed amount of Cu (qe) for the four sets of samples showing the pH effect on Cu adsorption, which decreases with decreasing the pH (Set 3 > Set 1 > Sets 2 and 4). A secondary contribution is given by the Na concentration. The Cu adsorption of Set 4 is higher than Set 2 (both pH 5); the significantly lower concentration of Na in Set 4 could enhance the adsorption of Cu. See Table 1 for specific details on the four sets of samples. Note that the samples with initial Cu concentration equal to zero are not plotted. The dashed line represents the copper hydroxide saturation at pH 6, calculated with PHREEQC and compared with the existing literature (Fu & Wang, 2011; Mirbagheri & Hosseini, 2005). (b) Adsorption of Na and Na + Cu. The Na adsorption appears strongly affected by both Cu concentration and pH.

4 Results and Discussion

We first present the geochemical data; Table 1 contains the saturating solution characteristics and Figure 5 shows the adsorption results. The observation that the Cu isotherms appear as straight lines in the log-log plot of Figure 5 suggests a Freundlich-type relation between solution concentration and the adsorbed Cu (Foo & Hameed, 2010). The Cu adsorption increases with increasing pH. The third set of samples, corresponding to pH adjusted at 6, shows the highest adsorption, while Sets 2 and 4, whose pH values were fixed at 5, reveal the lowest adsorption. The

first set, with variable (unadjusted) pH ranging between 5.08 and 5.66, has an intermediate behavior. The comparison between Sets 2 and 4 indicates a reduced Cu adsorption as consequence of the higher Na concentration. While the Na data also present some degree of regularity, they appear less aligned than the Cu isotherms. We interpret this difference to be associated with the weaker Na adsorption relative to Cu. The values of Na are probably more the result of the different Cu concentrations and pH conditions than the expression of Na adsorption affinity. As for Cu, Set 3 shows higher adsorption than Set 2. Sets 3 and 4, both with pH 6, show the expected alignment.

The chemical analyses performed for the adsorption experiments also highlighted the presence Ca ions due to desorption reactions in the solutions of Set 1. The Ca desorption increased as pH decreased, remaining negligible as the samples with lower pH also had the higher Cu concentrations (maximum Ca desorption 2.14 mg/L). However, we decided to wash the sand with acidic solution before sample preparation to exclude more significant desorption effects for the following sets, particularly for Set 4 because of its pH 5 and lower Cu and Na concentrations. We find that the above supports the usefulness of including chemical analyses in similar SIP investigations.

The adsorption results allow the calculation of the surface site occupancy for Cu and Na following equation 11. Multiplying the measured specific surface area (0.2 m^2/g, from Brunauer-Emmett-Teller) by the amount of sand used (1 kg) and dividing by the volume of solution (0.5 l), we obtain a surface area of 400 m^2/L. We can then calculate the number of sites using the previously discussed surface site density of 8 site/nm^2. A comparison with the adsorption results highlights that the site occupancies for Na and Cu range between 1 and 2.7%.

Figures 6 and 7 show the quadrature conductivity and phase response as a function of frequency for all four sets of samples. The SIP results show how the capacitive behavior of the saturated sand changes in response to the different chemical compositions of the pore fluid. Particular variations are visible within Set 1 (Figures 6a and 7a). Both the quadrature conductivity and the phase lag decrease from sample 1 to 10, as the amount of chalcanthite increases. Taking into account the effect of the dissolved chalcanthite on pH and solution conductivity (Table 1), we can also see how quadrature conductivity and phase lag decrease with decreasing pH and/or increasing solution conductivity.

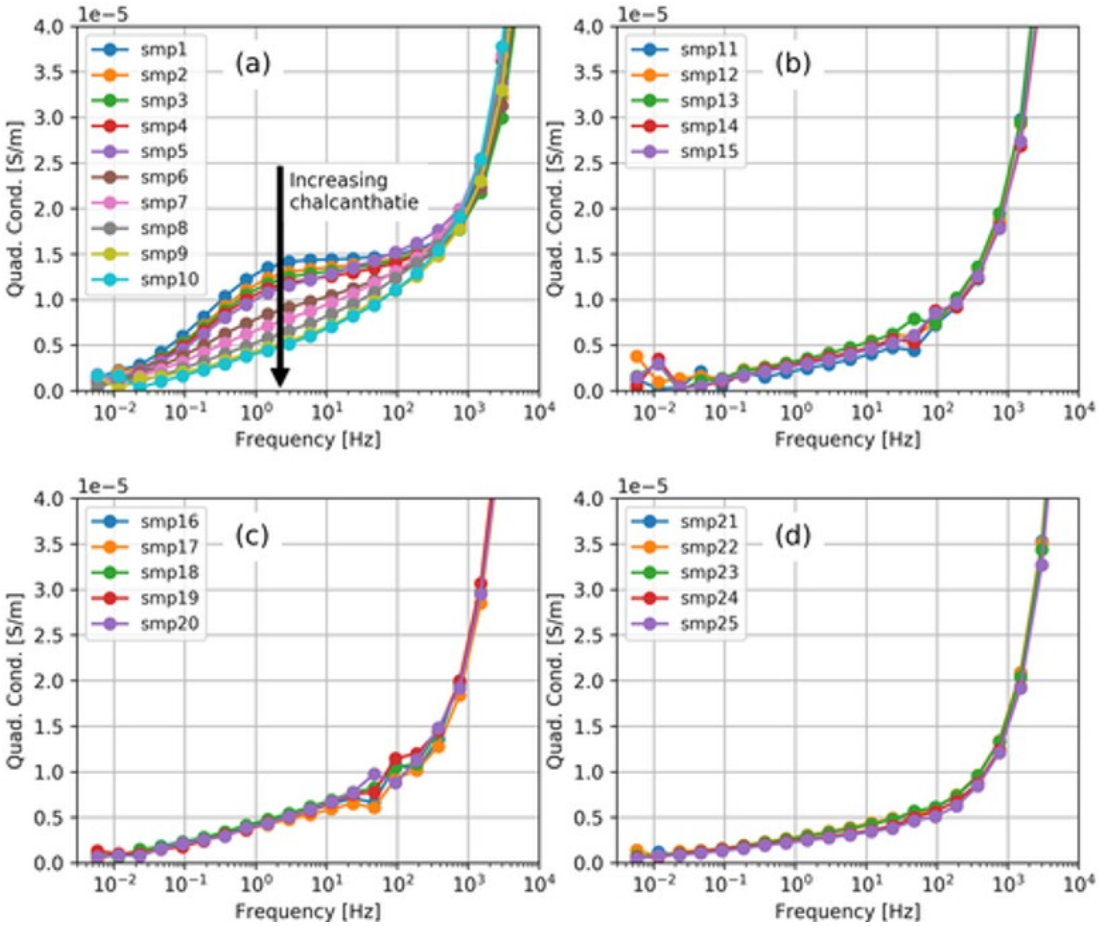

Figure 6

Quadrature conductivity spectra for the four sets of samples: (a) Set 1, nonadjusted pH and fluid conductivity; (b) Set 2, pH adjusted at 5 and fluid conductivity ≈ 500 µS/cm; (c) Set 3, pH adjusted at 6 and fluid conductivity at ≈ 500 µS/cm; and (d) Set 4, pH adjusted at 5 and fluid conductivity ≈ 170 µS/cm. Refer to Table 1 for details about the equilibrium solution composition and associated ion adsorption. The marker size corresponds to the estimated error (see section 3.2).

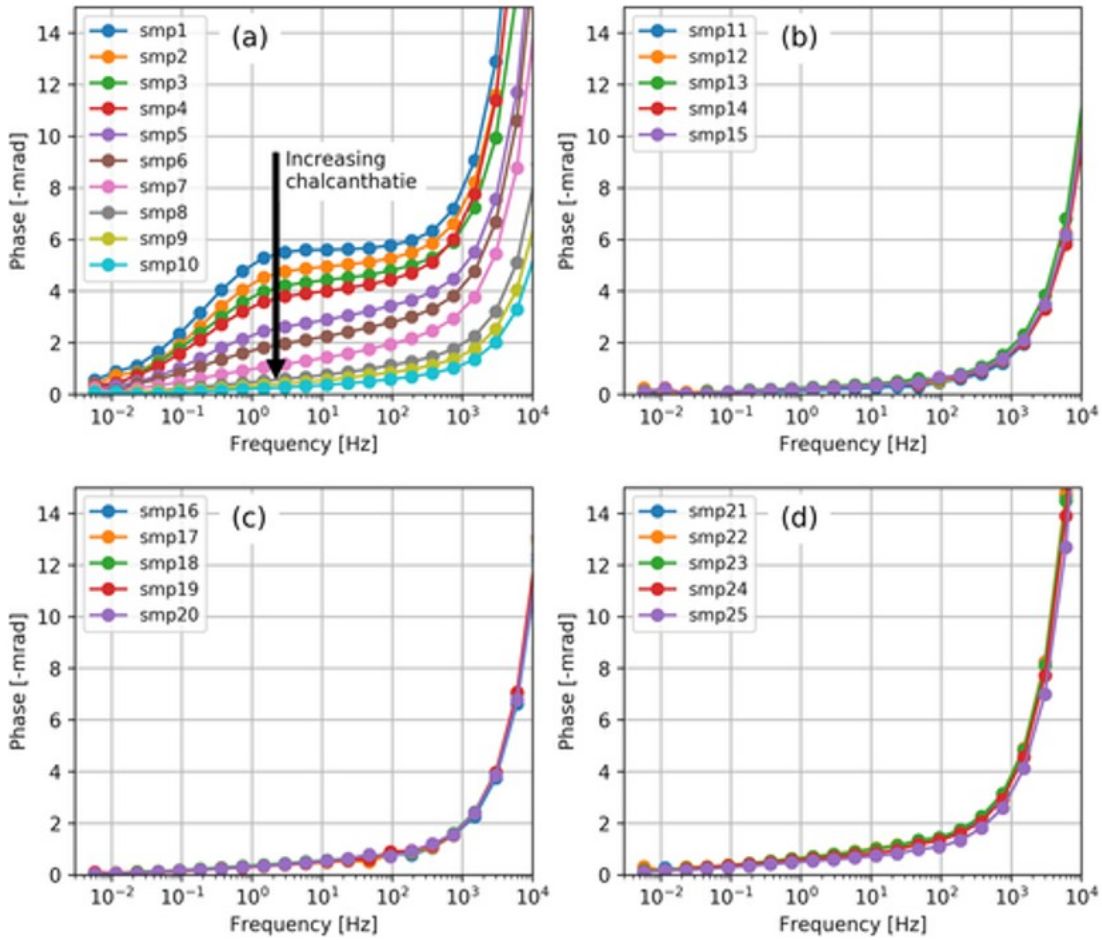

Figure 7

Phase spectra for the four sets of samples: (a) Set 1, nonadjusted pH and fluid conductivity; (b) Set 2, pH adjusted at 5 and fluid conductivity ≈ 500 µS/cm; (c) Set 3, pH adjusted at 6 and fluid conductivity at ≈ 500 µS/cm; and (d) Set 4, pH adjusted at 5 and fluid conductivity ≈ 170 µS/cm. Refer to Table 1 for details about the equilibrium solution composition and associated ion adsorption. The marker size corresponds to the estimated error (see section 3.2).

A more explicit illustration of the variations between the different samples of Set 1 is obtained by subtracting the spectrum of sample 10 from those of the other samples, which highlights the lowest values of quadrature conductivity (Figure 8a). Figure 8a allows us to observe how the polarization builds up with a characteristic frequency around 1 Hz, with no relevant variations below 5 mHz and over 200 Hz. We do not observe appreciable variations of characteristic polarization frequency when changing pore fluid, which is in line with previous studies that showed grain size and saturation are main determinants of the characteristic polarization frequency (Binley et al., 2005; Revil et al., 2015).

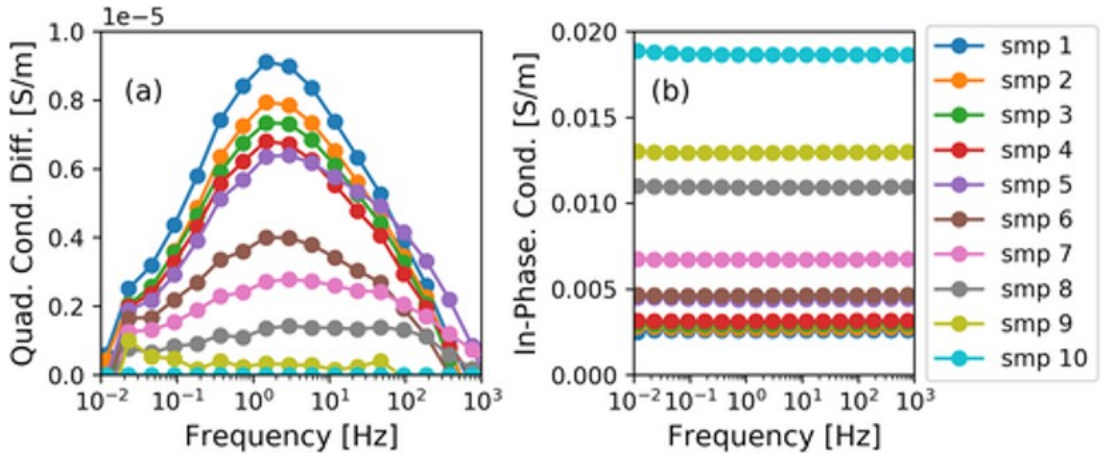

Figure 8

(a) Difference between the spectrum associated with each of the first nine in Set 1 and the spectrum of the tenth sample (e.g., Spectrum 1–Spectrum 10). The obtained spectra highlight how the changes in polarization are most significant near the frequency of 1 Hz, which is defined as main polarization frequency. Therefore, we can extract information near 1 Hz as representative of the whole spectrum and use it for more general and comprehensive interpretations involving different data sets (such as that shown in Figure 9). (b) In-phase conductivity of the 10 samples in Set 1.

Different from Set 1, the spectra of the other sets (2, 3, and 4) do not show significant changes within each set. Variations within these sets are smaller than 0.1 mrad, which is lower than the confidence limit of measurement for the SIP setup (as discussed above). However, some differences are visible between Sets 2, 3, and 4. The lower quadrature conductivities of Set 2 with respect to Set 3 (Figure 9a) suggests that, although strongly limited by the relatively high solution conductivity, the polarization of Set 3 remains higher due to higher pH (pH equal to 5 in 2, pH 6 in Set 3). That is, both pH and solution conductivity limit the polarization of Set 2 while the higher pH of Set 3 allows, to some degree, higher values of quadrature conductivity. However, the opposite case (i.e., the lower conductivity and pH 5 of Set 4), does not present the same increase of quadrature conductivity values. This suggests that at pH 5 the polarization is strongly limited and is independent of conductivity value (see position of Set 4 in Figure 9a). These explanations agree with what was previously observed in Set 1, but are based on smaller data differences, at the limit of the setup resolution. This is particularly the case for measurements taken over 1 kHz, where the error increases (see Figure 4) and where the effect of changing the fluid chemistry decreases (see Figure 8a). For this reason, we do not base our interpretation on this part of the spectra. We also find that new and more specific experiments are necessary in order to further investigate this subtle relevance difference between pH and solution conductivity.

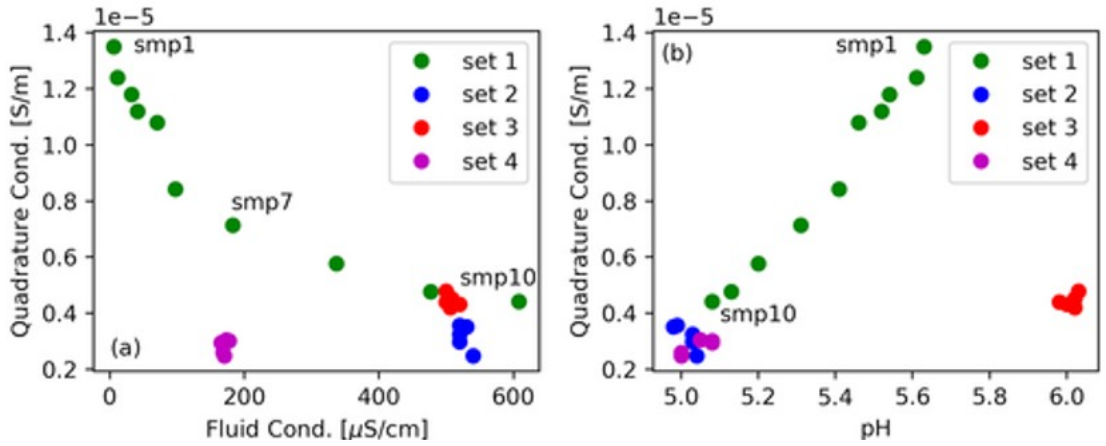

Figure 9

Quadrature conductivity at 1.46 Hz for the 25 samples plotted against the solution conductivity (a) and pH (b). The figure highlights the significant effect of the pH and solution conductivity on the SIP response of the saturated silica sand. While small changes of the quadrature conductivity are associated with the adsorption and substitution of Na and Cu. See Table 1 for sample details. SIP = spectral induced polarization.

Figures 9 and 10 offer a better overall assessment of the SIP responses. Figure 9 shows the quadrature conductivity values at the characteristic polarization frequency of 1.46 Hz. The signal changes at the characteristic frequency reveal a decrease in quadrature conductivity with increasing fluid conductivity (Figure 9a) and/or decreasing pH (Figure 9b). The figure shows that Set 4 in Figure 9a and Set 3 in Figure 9b are out of trend with the other results, highlighting that both pH and solution conductivity affect the SIP response. In Figure 9a, for example, despite the low fluid conductivity values of Set 4 (≈ 185 μS/cm, comparable with sample 7), the responses are significantly out of trend, showing lower quadrature conductivity values. Similarly, Set 2 shows lower values of quadrature conductivity than other samples with similar fluid conductivity (Set 3 and samples 9 and 10). These observations indicate that the effect of pH and fluid conductivity were actually superimposed on the samples of Set 1. Figures 9 and 10 also confirm the relatively smaller sensitivity of SIP signals associated with a change in the ion type (i.e., when substituting chalcanthite and halite). Figure 9a also shows that because of the decay-like trend of the phase, the variation of 40 μS/cm between Sets 2 and 3 has a negligible effect due to the overall high solution conductivity.

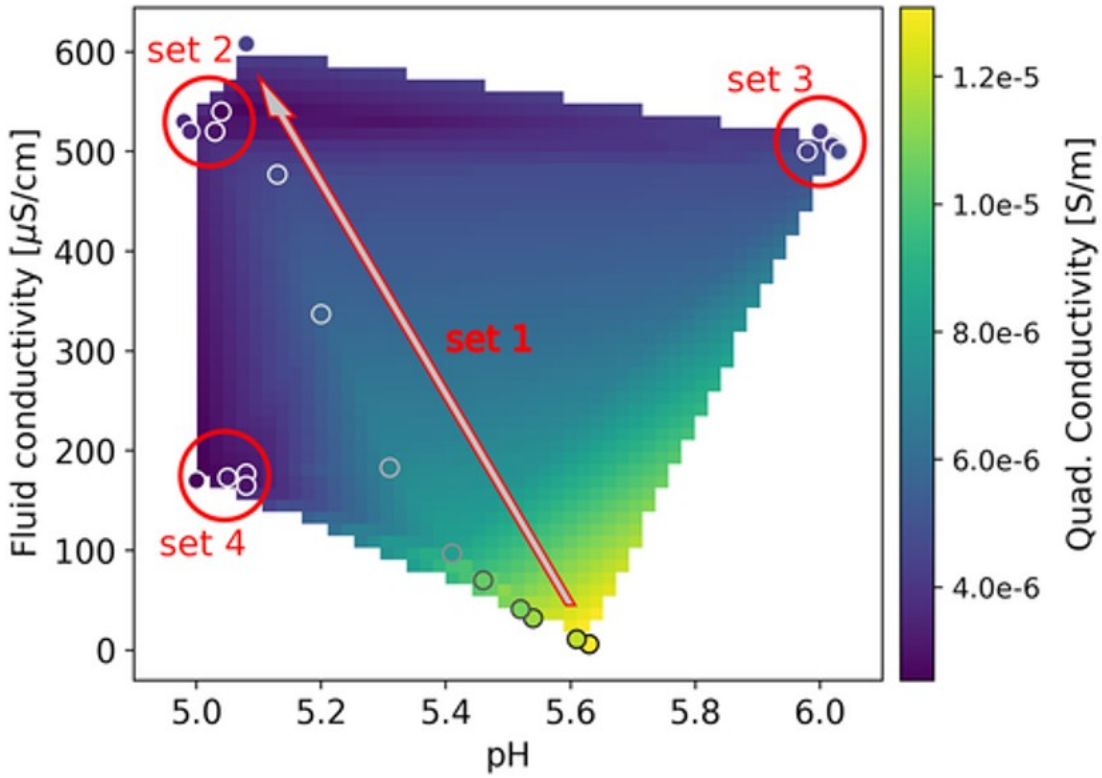

Figure 10

Linear interpolation of the quadrature conductivity values at 1.46 Hz as a function of solution conductivity and pH. The arrow follows the values of Set 1 from Samples 1 to 10. The figure highlights the primary effect of pH and solution conductivity on the measured quadrature conductivity values, while no significant variations are associated with the Cu-Na substitution (Sets 2, 3, and 4). Refer to Table 1 for details on pore fluid composition and associated adsorption results.

Analogous observations can be made based on phase-lag values. However, because the solution conductivity was investigated over a wide range of values (10 to 600 µS/cm), there is a strong variation of the real component of the conductivity (see resistivity values in Table 1and Figure 8b). For this reason, we focus on the quadrature conductivity, which offers more direct insight into the capacitive response of the samples.

On the basis of our results, the predominant contributions to the SIP response become evident. The polarization decreases with decreasing pH, which is physically explainable considering the neutralization of the surface charge due to the protonation of the silanol groups. The polarization decreases with increasing pore fluid conductivity, an observation that is explainable considering the higher ionic strength and consequent fluid capacity of shielding the surface charge. We also recognize that the spectra do not show significant variations when pH and solution conductivity are fixed and only the ratio between halite and chalcanthite is changed (Sets 2, 3, and 4).

The insensitivity of the SIP measurements to the Cu/Na concentration ratio is interpreted to be associated with the small resulting fraction of sites involved

in the cation adsorption. Additionally, relatively low capacitive responses were measured (phase lag values ranging between 6 and 0.25 mrad). The combination of these two factors may explain why the Cu-Na substitution does not cause appreciable variations of the SIP response. It is worth noting that previous works reporting variations of the SIP response associated with the dissolved salt type may have been affected by the pH variation as only the solution conductivity was kept constant. For example, see the SIP response changes associated with the NaCl-$CuSO_4$substitution and the reported pH values in Vaudelet et al. (2011b, their Figure 6 and Table 3); and similarly, see the SIP response and pH changes associated with the NaCl-$ZnSO_4$substitution in Vaudelet et al. (2011a, their Figure 5 and Table 3). Consequently, the reported changes of the phase lag values are more likely due to the pH change than to the ion type. Even with negligible adsorption of anions, it is also evident that the anionic species in solution may affect SIP response by changing the pH due to different hydrolysis intensity. Different salts of the same cation could have different effects on SIP signals.

The low site-occupancy densities associated with our experiments also suggest the effect of pH and ionic strength to have different causes rather than the adsorption changes associated with pH and ionic strength changes. Namely, the pH would not affect the SIP signals because of a significant difference in the cation adsorption (which the pH contributes to determine). And similarly, the ionic strength effect would be unrelated to its control on the adsorption equilibrium, that is, the effect of the ions on the SIP response does not involve a removal of the same ions from the solution.

Regarding the surface site-occupancy densities, our values well agree with the ones obtained from X-ray photon spectroscopy by Skold et al., 2011 (see their Figure 1a). This suggests that the adsorption experiment approach, which enabled the calculation of the site occupancies from chemical analysis of the supernatant solutions, could be used to obtain information that has been in the past obtained using more expensive X-ray photon spectroscopy approaches. On the basis of our findings, we highlight how such a solution could readily play an important role in the development of new mechanistic and empirical SIP models by contributing to the calibration of the underlying complexation models and/or validating the sensitivity of the SIP method to the specific investigated field variables.

Our results agree with the theoretical model by Skold et al., 2011, which requires consideration of the contribution of the protonation reactions at the silica/water interface on surface conductivity (see quadrature variation as a function of the pH, their Figure 1b). Complementing their theory, our extensive laboratory-based investigations experimentally document proton adsorption and the consequent influence on the SIP signal. In addition to the concurrence between existing theory and new experimental results, for the first time, our joint investigation of pH, solution conductivity, and dissolved ion type explores the mutual influence of these variables on the SIP response. While the low Cu and Na site occupancies explain the absence of

effects from the ion type, a significant reciprocal influence is observed between pH and fluid conductivity. For example, Figure 9a shows how the pH effect is higher at lower fluid conductivity. Our research generally highlights the importance of accounting for the reciprocal influence of the geochemical variables when studying their effect on the SIP signature.

5 Conclusions

We performed laboratory experiments to explore the sensitivity of SIP method to variations in composition of the saturating solution in silica sands, specifically pH, fluid conductivity, and ion type. We also measured the adsorption associated with the different pore fluids. We found that the effects of pH and solution conductivity (interpreted above as a proxy for the ionic strength) dominate the SIP signals. Meanwhile, no variations were associated with the Na-Cu substitution. The low site occupancies obtained from the adsorption experiments likely explain the insensitivity to ion adsorption and substitution and suggest that the effect of ionic strength and pH is unrelated to their control on ion adsorption. The explored values of ionic strength significantly modified the SIP response. We found that higher salinity values could potentially enhance the ion adsorption but that their effect on SIP signals may remain secondary (negligible) if associated with an increase of the ionic strength, as expected on the basis of the adsorption equilibria. Furthermore, higher pore fluid conductivity would decrease the phase values and hinder the acquisition of interpretable SIP data sets.

Previous works have noted the impact of changing the type of salts on the SIP response of saturated silica sand (Revil & Skold, 2011; Vaudelet et al., 2011a, 2011b; Weller et al., 2011). The commonly accepted interpretation of the SIP response is that the different ion adsorption behavior (caused by different ionic radius, charge, hydration, etc.) influences the EDL electrochemical state and, consequently, the SIP capacitive response. For the first time, our results highlight the potentially dominant effect of pH and solution conductivity on the SIP response and the importance of joint consideration of the saturating fluid and interfacial geochemistry when interpreting the SIP response.

Albeit a challenge, a significant opportunity exists to translate laboratory-developed SIP-based approaches to quantify adsorption and other geochemical factors for field applications. A key obstacle is that the SIP signature is also sensitive to a range of other subsurface properties, such as lithology, organic content, and saturation, which are naturally heterogeneous. The overall effect of these additional factors on SIP signatures may disguise the SIP signature associated with pore fluid conductivity, pH, and ion type, making it difficult to deconvolute from other influences. Time-lapse field SIP approaches may mitigate some of these challenges, as it in effect can “remove” the SIP signature associated with lithology and organic matter, offering the potential to highlight geochemical changes. While the concentration ranges that we explored cover the

common natural conditions, new laboratory investigations are needed to address how our findings would differ with different types of adsorbents.

Acknowledgments

The authors thank David L. Parkhurst (U.S. Geological Survey) for his availability and contribution to the PHREEQC modeling. Luca Peruzzo and Myriam Schmutz gratefully acknowledge the financial support from IDEX (Initiative D'EXellence, France) and the European Regional Development Fund Interreg Sudoe - soil take care SOE1/P4/F0023 - Sol Precaire. Yuxin Wu acknowledges the support of ARPA-E ROOTS (Advanced Research Projects Agency - Energy, Rhizosphere Observations Optimizing Terrestrial Sequestration, Lawrence Berkeley National Laboratory). Susan Hubbard acknowledges the support of the Watershed Function Scientific Focus Area, which is funded to Berkeley Lab by the U.S. Department of Energy, Office of Science, Office of Biological and Environmental Research under award DE-AC02-05CH11231. SIP complete spectra are available at this https://doi.org/10.5281/zenodo.1174370 repository.

References

Abdulsamad, F., Florsch, N., Schmutz, M., & Camerlynck, C. (2016). Assessing the high frequency behavior of non-polarizable electrodes for spectral induced polarization measurements. *Journal of Applied Geophysics*, 135, 449– 455. https://doi.org/10.1016/j.jappgeo.2016.01.001

Abrol, I. P., Yadav, J. S. P., & Massaoud, F. I. (1988). Salt-affected soils and their management. Retrieved from http://www.fao.org/docrep/x5871e/x5871e00.htm#Contents

Atekwana, E., & Slater, L. D. (2009). Biogeophysics: A new frontier in Earth science research. *Reviews of Geophysics*, 47, RG4004. https://doi.org/10.1029/2009RG000285

Awan, M. A., Qazi, I. A., & Khalid, I. (2003). Removal of heavy metals through adsorption using sand. *Journal of Environmental Sciences*, 15(3), 413– 416.

Behrens, S. H., & Grier, D. G. (2001). The charge of glass and silica surfaces. *The Journal of Chemical Physics*, 115(14), 6716– 6721. https://doi.org/10.1063/1.1404988

Binley, A. (2013). R3t, version 1.8. Lancaster University.

Binley, A., Hubbard, S. S., Huisman, J. A., Revil, A., Robinson, D. A., Singha, K., & Slater, L. D. (2015). The emergence of hydrogeophysics for improved understanding of subsurface processes over multiple scales. *Water Resources Research*, 51, 1– 30. https://doi.org/10.1002/2015WR017016

Binley, A., Slater, L. D., Fukes, M., & Cassiani, G. (2005). Relationship between spectral induced polarization and hydraulic properties of saturated and unsaturated sandstone. *Water Resources Research*, 41, W12417. https://doi.org/10.1029/2005WR004202

Bradl, H. B. (2004). Adsorption of heavy metal ions on soils and soils constituents. *Journal of Colloid and Interface Science*, 277(1), 1– 18. https://doi.org/10.1016/j.jcis.2004.04.005

Brun, L. A., Maillet, J., Hinsinger, P., & Pepin, M. (2001). Evaluation of copper availability to plants in copper-contaminated vineyard soils. *Environmental Pollution*, 111(2), 293– 302. https://doi.org/10.1016/S0269-7491(00)00067-1

Brun, L. A., Maillet, J., Richarte, J., Herrmann, P., & Remy, J. C. (1998). Relationships between extractable copper, soil properties and copper uptake by wild plants in vineyard soils. *Environmental Pollution*, 102(2-3), 151– 161. https://doi.org/10.1016/S0269-7491(98)00120-1

Butt, H.-J., Graf, K., & Kappl, M. (2004). Thermodynamics of interfaces. *Physics and Chemistry of Interfaces*, 26– 41.

Chen, J., Hubbard, S. S., & Williams, K. H. (2013). Data-driven approach to identify field-scale biogeochemical transitions using geochemical and geophysical data and hidden Markov models: Development and application at a uranium-contaminated aquifer. *Water Resources Research*, 49, 6412–6424. https://doi.org/10.1002/wrcr.20524

Chen, J., Hubbard, S. S., Williams, K. H., Flores Orozco, A., & Kemna, A. (2012). Estimating the spatiotemporal distribution of geochemical parameters associated with biostimulation using spectral induced polarization data and hierarchical Bayesian models. *Water Resources Research*, 48, W05555. https://doi.org/10.1029/2011WR010992

Dove, P. M., & Craven, C. M. (2005). Surface charge density on silica in alkali and alkaline earth chloride electrolyte solutions. *Geochimica et Cosmochimica Acta*, 69(21), 4963– 4970. https://doi.org/10.1016/j.gca.2005.05.006

Echeverria, J. C., Morera, M. T., Mazkiaran, C., & Garrido, J. J. (1998). Competitive sorption of heavy metal by soils. Isotherms and fractional factorial experiments. *Environmental Pollution*, 101(2), 275– 284. https://doi.org/10.1016/S0269-7491(98)00038-4

Feng, M.-H., Shan, X.-Q., Zhang, S., & Wen, B. (2005). A comparison of the rhizosphere-based method with DTPA, EDTA, CaCl 2, and NaNO 3 extraction methods for prediction of bioavailability of metals in soil to barley. *Environmental Pollution*, 137(2), 231– 240. https://doi.org/10.1016/j.envpol.2005.02.003

Foo, K., & Hameed, B. H. (2010). Insights into the modeling of adsorption isotherm systems. *Chemical Engineering Journal*, 156(1), 2– 10. https://doi.org/10.1016/j.cej.2009.09.013

Fu, F., & Wang, Q. (2011). Removal of heavy metal ions from wastewaters: A review. *Journal of Environmental Management*, 92(3), 407– 418. https://doi.org/10.1016/j.jenvman.2010.11.011

Fuller, B. D., & Ward, S. H. (1970). Linear system description of the electrical parameters of rocks. *IEEE Transactions on Geoscience Electronics*, 8(1), 7– 18. https://doi.org/10.1109/TGE.1970.271447

Gupta, S. S., & Bhattacharyya, K. G. (2011). Kinetics of adsorption of metal ions on inorganic materials: A review. *Advances in Colloid and Interface Science*, 162(1-2), 39– 58. https://doi.org/10.1016/j.cis.2010.12.004

Hiemstra, T., De Wit, J. C. M., & Van Riemsdijk, W. H. (1989). Multisite proton adsorption modeling at the solid/solution interface of (hydr)oxides: A new approach. *Journal of Colloid and Interface Science*, 133(1), 105– 117. https://doi.org/10.1016/0021-9797(89)90285-3

Hiemstra, T., & Van Riemsdijk, W. H. (1996). A surface structural approach to ion adsorption: The charge distribution (CD) model. *Journal of Colloid and Interface Science*, 179(2), 488– 508. https://doi.org/10.1006/jcis.1996.0242

Hiemstra, T., & Van Riemsdijk, W. H. (1999). Surface structural ion adsorption modeling of competitive binding of oxyanions by metal (hydr) oxides. *Journal of Colloid and Interface Science*, 210(1), 182– 193. https://doi.org/10.1006/jcis.1998.5904

Hiemstra, T., Van Riemsdijk, W. H., & Bolt, G. H. (1989). Multisite proton adsorption modeling at the solid/solution interface of (hydr) oxides: A new approach: I. Model description and evaluation of intrinsic reaction constants. *Journal of Colloid and Interface Science*, 133(1), 91– 104. https://doi.org/10.1016/0021-9797(89)90284-1

Hooda, P. S. (2010). *Trace elements in soils*. Chichester, West Sussex, UK: Wiley Online Library. https://doi.org/10.1002/9781444319477

Hubbard, S. S., Williams, K., Conrad, M. E., Faybishenko, B., Peterson, J., Chen, J., et al. (2008). Geophysical monitoring of hydrological and biogeochemical transformations associated with Cr(VI) bioremediation. *Environmental Science and Technology*, 42(10), 3757– 3765. https://doi.org/10.1021/es071702s

Icenhower, J. P., & Dove, P. M. (2000). The dissolution kinetics of amorphous silica into sodium chloride solutions: Effects of temperature and ionic strength. *Geochimica et Cosmochimica Acta*, 64(24), 4193– 4203. https://doi.org/10.1016/S0016-7037(00)00487-7

Järup, L. (2003). Hazards of heavy metal contamination. *British Medical Bulletin*, 68(1), 167– 182. https://doi.org/10.1093/bmb/ldg032

Kemna, A., Binley, A., Cassiani, G., Niederleithinger, E., Revil, A., Slater, L., et al. (2012). An overview of the spectral induced polarization method for near-surface applications. *Near Surface Geophysics*, 10(6), 453– 468.

Kremer, T., Schmutz, M., Maineult, A., & Agrinier, P. (2016). Laboratory monitoring of CO_2 injection in saturated silica and carbonate sands using

spectral induced polarization. *Geophysical Journal International*, 207(2), 1258– 1272. https://doi.org/10.1093/gji/ggw333

Lander, L., & Reuther, R. (2004). Metals in society and in the environment: A critical review of current knowledge on fluxes, speciation, bioavailability and risk for adverse effects of copper, chromium, nickel and zinc. *Environmental Pollution*, 8, 0– 406.

Leamson, R. N., Josephus Thomas, J., & EHrlinger, H. P. III (1969). A study of surface areas of particulate microcrystalline silica and silica sand. *Illinois State Geological Survey*, 444, 1– 12.

Leroy, P., & Revil, A. (2004). A triple-layer model of the surface electrochemical properties of clay minerals. *Journal of Colloid and Interface Science*, 270(2), 371– 380. https://doi.org/10.1016/j.jcis.2003.08.007

Leroy, P., Revil, A., Kemna, A., Cosenza, P., & Ghorbani, A. (2008). Complex conductivity of water-saturated packs of glass beads. *Journal of Colloid and Interface Science*, 321(1), 103– 117. https://doi.org/10.1016/j.jcis.2007.12.031

McBride, M. B. (1994). *Environmental chemistry of soils*. Oxford, UK: Oxford University Press.

McLaren, R. G., Williams, J. G., & Swift, R. S. (1981). The adsorption of copper by soil materials at low equilibrium solution concentrations. *Journal of Soil Science*, 32(2), 247– 256. https://doi.org/10.1111/j.1365-2389.1981.tb01704.x

Milonjić, S. K. (2007). A consideration of the correct calculation of thermodynamic parameters of adsorption. *Journal of the Serbian Chemical Society*, 72(12), 1363– 1367. https://doi.org/10.2298/JSC0712363M

Mirbagheri, S. A., & Hosseini, S. N. (2005). Pilot plant investigation on petrochemical wastewater treatment for the removal of copper and chromium with the objective of reuse. *Desalination*, 171(1), 85– 93. https://doi.org/10.1016/j.desal.2004.03.022

Parkhurst, D. L., & Appelo, C. A. J. (2013). Description of input and examples for PHREEQC version 3—A computer program for speciation, batch-reaction, one-dimensional transport, and inverse geochemical calculations: U.S. Geological Survey Techniques and Methods (book 6, chap. A43, 497 pp.). Denver, CO: U.S. Geological Survey. Retrieved from https://pubs.usgs.gov/tm/06/a43/

Pauling, L. (1929). The principles determining the structure of complex ionic crystals. *Journal of the American Chemical Society*, 51(4), 1010– 1026. https://doi.org/10.1021/ja01379a006

Plettinck, S., Chou, L., & Wollast, R. (1994). Kinetics and mechanisms of dissolution of silica at room temperature and pressure. *Mineralogical Magazine A*, 58, 728– 729.

Porus, M., Labbez, C., Maroni, P., & Borkovec, M. (2011). Adsorption of monovalent and divalent cations on planar water-silica interfaces studied by optical reflectivity and Monte Carlo simulations. *The Journal of Chemical Physics*, 135(6), 064701. https://doi.org/10.1063/1.3622858

Rahnemaie, R., Hiemstra, T., & van Riemsdijk, W. H. (2006). Inner- and outer-sphere complexation of ions at the goethite-solution interface. *Journal of Colloid and Interface Science*, 297(2), 379– 388. https://doi.org/10.1016/j.jcis.2005.11.003

Revil, A. (1999). Ionic diffusivity, electrical conductivity, membrane and thermoelectric potentials in colloids and granular porous media: A unified model. *Journal of Colloid and Interface Science*, 212(2), 503– 522. https://doi.org/10.1006/jcis.1998.6077

Revil, A. (2013). Effective conductivity and permittivity of unsaturated porous materials in the frequency range 1 mHz–1 GHz. *Water Resources Research*, 49, 306– 327. https://doi.org/10.1029/2012WR012700

Revil, A., Binley, A., Mejus, L., & Kessouri, P. (2015). Predicting permeability from the characteristic relaxation time and intrinsic formation factor of complex conductivity spectra. *Water Resources Research*, 51, 6672– 6700. https://doi.org/10.1002/2015WR017074

Revil, A., & Florsch, N. (2010). Determination of permeability from spectral induced polarization in granular media. *Geophysical Journal International*, 181(3), 1480– 1498.

Revil, A., Mendonça, C. A., Atekwana, E. A., Kulessa, B., Hubbard, S. S., & Bohlen, K. J. (2010). Understanding biogeobatteries: Where geophysics meets microbiology. *Journal of Geophysical Research*, 115, G00G02. https://doi.org/10.1029/2009JG001065

Revil, A., & Skold, M. (2011). Salinity dependence of spectral induced polarization in sands and sandstones. *Geophysical Journal International*, 187(2), 813– 824. https://doi.org/10.1111/j.1365-246X.2011.05181.x

Rubin, Y., & Hubbard, S. S. (2005). *Hydrogeophysics* (Vol. 50). Dordrecht, Netherlands: Springer Science & Business Media.

Schmutz, M., Revil, A., Vaudelet, P., Batzle, M., Viñao, P. F., & Werkema, D. D. (2010). Influence of oil saturation upon spectral induced polarization of oil-bearing sands. *Geophysical Journal International*, 183(1), 211– 224. https://doi.org/10.1111/j.1365-246X.2010.04751.x

Skold, M., Revil, A., & Vaudelet, P. (2011). The pH dependence of spectral induced polarization of silica sands: Experiment and modeling. *Geophysical Research Letters*, 38, L12304. https://doi.org/10.1029/2011GL047748

Stumm, W. (1992). *Chemistry of the solid-water interface: Processes at the mineral-water and particle-water interface in natural systems*. John Wiley & Son Inc.

Sverjensky, D. A., & Sahai, N. (1996). Theoretical prediction of single-site surface-protonation equilibrium constants for oxides and silicates in water. *Geochimica et Cosmochimica Acta*, 60(20), 3773– 3797. https://doi.org/10.1016/0016-7037(96)00207-4

Tadros, T. F., & Lyklema, J. (1969). The electrical double layer on silica in the presence of bivalent counter-ions. *Journal of Electroanalytical Chemistry and Interfacial Electrochemistry*, 22(1), 1– 7. https://doi.org/10.1016/S0022-0728(69)80140-3

Tarasov, A., & Titov, K. (2007). Relaxation time distribution from time domain induced polarization measurements. *Geophysical Journal International*, 170(1), 31– 43. https://doi.org/10.1111/j.1365-246X.2007.03376.x

Titov, K., Kemna, A., Tarasov, A., & Vereecken, H. (2004). Induced polarization of unsaturated sands determined through time domain measurements. *Vadose Zone Journal*, 3(4), 1160– 1168. https://doi.org/10.2136/vzj2004.1160

Titov, K., Komarov, V., Tarasov, V., & Levitski, A. (2002). Theoretical and experimental study of time domain-induced polarization in water-saturated sands. *Journal of Applied Geophysics*, 50(4), 417– 433. https://doi.org/10.1016/S0926-9851(02)00168-4

Vaudelet, P., Revil, A., Schmutz, M., Franceschi, M., & Bégassat, P. (2011a). Changes in induced polarization associated with the sorption of sodium, lead, and zinc on silica sands. *Journal of Colloid and Interface Science*, 360(2), 739– 752. https://doi.org/10.1016/j.jcis.2011.04.077

Vaudelet, P., Revil, A., Schmutz, M., Franceschi, M., & Bégassat, P. (2011b). Induced polarization signatures of cations exhibiting differential sorption behaviors in saturated sands. *Water Resources Research*, 47, W02526. https://doi.org/10.1029/2010WR009310

Vereecken, H., Binley, A., Cassiani, G., Revil, A., & Titov, K. (2006). *Applied Hydrogeophysics*. Dordrecht, Netherlands: Springer. https://doi.org/10.1007/978-1-4020-4912-5

Vlasova, N. N. (2000). Adsorption of Cu 2+ ions onto silica surface from aqueous solutions containing organic substances. *Colloids and Surfaces A: Physicochemical and Engineering Aspects*, 163(2-3), 125– 133. https://doi.org/10.1016/S0927-7757(99)00299-X

Vuceta, J. (1976). *Adsorption of Pb (II) and Cu (II) on alfa-quartz from aqueous solution: influence of pH, ionic strength, and complexing ligands*. Pasadena, CA: California Institute of Technology.

Weerasooriya, R., Aluthpatabendi, D., & Tobschall, H. J. (2001). Charge distribution multi-site complexation (CD-MUSIC) modeling of Pb (II) adsorption on gibbsite. *Colloids and Surfaces A: Physicochemical and Engineering Aspects*, 189(1-3), 131– 144. https://doi.org/10.1016/S0927-7757(01)00578-7

Weerasooriya, R., Wijesekara, H., & Bandara, A. (2002). Surface complexation modeling of cadmium adsorption on gibbsite. *Colloids and Surfaces A: Physicochemical and Engineering Aspects*, 207(1-3), 13– 24. https://doi.org/10.1016/S0927-7757(02)00004-3

Weller, A., Breede, K., Slater, L., & Nordsiek, S. (2011). Effect of changing water salinity on complex conductivity spectra of sandstones. *Geophysics*, 76(5), F315– F327. https://doi.org/10.1190/geo2011-0072.1

Weller, A., & Slater, L. (2012). Salinity dependence of complex conductivity of unconsolidated and consolidated materials: Comparisons with electrical double layer models. *Geophysics*, 77(5), D185– D198. https://doi.org/10.1190/geo2012-0030.1

Wu, Y., Hubbard, S., Williams, K. H., & Ajo-Franklin, J. (2010). On the complex conductivity signatures of calcite precipitation. *Journal of Geophysical Research*, 115, G00G04. https://doi.org/10.1029/2009JG001129

Yates, D. E., Levine, S., & Healy, T. W. (1974). Site-binding model of the electrical double layer at the oxide/water interface. *Journal of the Chemical Society, Faraday Transactions 1: Physical Chemistry in Condensed Phases*, 70(0), 1807– 1818. https://doi.org/10.1039/f19747001807

Zhu, B., & Alva, A. K. (1993). Differential adsorption of trace metals by soils as influenced by exchangeable cations and ionic strength. *Soil Science*, 155(1), 61– 66. https://doi.org/10.1097/00010694-199301000-00009